Journal of Casting & Materials Engineering Special Issue (2026) 1–6
https://doi.org/10.7494/jcme.2026.10.S1.1-6

The Impact of Wall Thickness on the Microstructure and Mechanical Properties of Austenitic High-Nickel Ductile Iron

Magdalena Bork[a], **Marcin Górny**[a*], **Giuliano Angella**[b], **Jan Marosz**[a]

[a] AGH University of Krakow, Faculty of Foundry Engineering, 30 Mickiewicza Av., 30-059 Kraków, Poland
[b] Research Institute CNR-ICMATE, via R. Cozzi 53, 20125 Milan, MI, Italy
e-mail: mgorny@agh.edu.pl

Received: 9 January 2026/Accepted: 16 February 2026/Published online: 16 March 2026
This article is published with open access at AGH University of Science and Technology Journals

Abstract

Austenitic ductile iron belongs to the cast iron group characterized by high nickel content, ranging from 18% to 36% by weight, which allows the formation of an austenitic metallic matrix. As a consequence, this cast iron group exhibits a combination of highly beneficial properties allowing utilization under extreme conditions and justifies the increased price of these cast iron grades. Some of the applications require complex castings with changing geometry and wall thicknesses. For this reason, the main objective of this study was to determine the possibility of obtaining castings with various degrees of wall thickness, including thin-walled: 3 mm, 5 mm, 13 mm and 25 mm, and good quality microstructures without defects as well as with mechanical properties on a similar level. For our investigations the austenitic ductile cast iron grade EN-GJSA-XNi22 was selected. Material characterization was carried out using optical microscopy, and static tensile test measurements. Additionally, the thermal analysis during crystallization was also determined. The investigations showed the highly homogeneous mechanical properties of castings with various wall thicknesses. The main differences in the microstructure parameters concerned the number and diameter of the graphite nodules.

Keywords:

Ni-Resist ductile iron, thin-walled castings, microstructures, static tensile test, thermal analysis

1. INTRODUCTION

Cast iron is one the most widely used foundry alloys due to its good balance between cost-effectiveness and desirable properties. Nowadays, the demand for advanced materials is continuously increasing, a fact driven by the need to operate materials under extreme conditions. For some of these purposes, high-nickel austenitic cast iron may be a viable solution.

High-nickel ductile cast iron, belonging to the group of Ni-Resist cast iron, is characterized by a nickel content of 18–36 wt.% and treatment with magnesium to form nodular graphite [1]. A nickel content >18% allows stable austenite to be obtained because the transformation from austenite (γ) to ferrite (α) does not occur [2, 3]. The combination of the austenitic metallic matrix and nodular graphite results in beneficial properties such as high ductility, improved mechanical properties, improved corrosion resistance and a wide range of service temperatures, including cryogenic conditions [4–6]. Thanks to these properties, high-nickel ductile iron is used in various applications ranging from chemical processing (cryogenic equipment), the electrical power industry (non-magnetic housings), internal combustion engines (exhaust manifolds) and others [6].

This study examines the possibility of obtaining castings with various wall thicknesses, including thin-walled, and 3–25 mm, with good quality microstructures and mechanical properties across the entire cross-section of wall thicknesses. For this investigation, the high-nickel austenitic ductile iron grade EN GJSA XNi22 was chosen. Castings were examined using optical microscopy to determine microstructural parameters such as graphite percentage, mean diameter and number of particles per 1 mm^2 and degree of spheroidization. To determine the mechanical properties, the tensile test was also carried out.

2. METHODS

2.1. Alloy preparation

For melt preparation an electrical induction furnace IMSK 10 (Inducal Göllingen, Dresden, Germany) of intermediate frequency with a 15-kg-capacity crucible (Mammut, Puschwitz, Germany) was used. One chemical composition, based on EN GJSA XNi22 was prepared, where the charge consisted of sorel metal, steel scrap, pure nickel, technically pure silica and Fe-Mn.

The melt was superheated to 1490 °C and held at this temperature for 2 min. Next, the spheroidization and inoculation processes were carried out using the bell method. Then, the melt was placed in the furnace again for 2 min. The liquid metal was poured into a mold to obtain Y block ingots with plate thicknesses 3 mm, 5 mm, 13 mm and 25 mm at the bottom end, at a temperature of approximately 1400°C.

2.2. Thermal analysis

The phase diagram of the investigated alloy was calculated using Thermo-Calc 2019a (TCFE7 database), enabling the estimation of phase volume fractions and phase transformation temperatures. For thermal analysis, the crystallization and cooling curves were recorded during preparation of the castings with Agilent 34970A.

2.3. Microstructure analysis

A Leica MEF 4M microscope and a QWin v3.5 quantitative analyzer were used for the metallographic analysis. The parameters which were analyzed are the following: graphite fraction, number of graphite nodules per 1 mm^2 of iron casting surface, nodularity acc. to ISO 945-1 and mean diameter of graphite nodules. Additionally, after etching with Stead's reagent, the secondary dendrite arm spacing (SDAS) as well as the number of columnar grains (dendrites) per unit length N_L were determined.

2.4. Tensile test

Static tensile tests at a constant strain rate were performed on a Zwick Roell AllroundLine Z10 testing system, equipped with a 10 kN load cell (class 0.5) and a dedicated specimen holder. A non-contact strain evaluation, a high-precision LaserXtens HP1-15 speckle-type laser extensometer (class 0.5), coupled with optical cameras, was employed. The applied strain rate was 6.4 × 10^{-3} s^{-1}. Mechanical properties such as yield strength ($R_{p0.2}$), ultimate tensile strength (R_m), and elongation (A) were automatically extracted from the obtained stress–strain curves using the testXpert II software package (ZwickRoell).

3. RESULTS AND DISCUSSION

3.1. Chemical composition

The chemical composition of the experimental cast iron is presented in Table 1. The carbon equivalent (CE) was calculated using the formula [7]:

$$CE = C\% + 0.33 \cdot Si\% + 0{,}047 \cdot Ni\% - (0.0055 \cdot Ni\% \cdot Si\%)$$

where C, Si and Ni denote the carbon, silicon and nickel contents, respectively [wt.%].

The chemical composition of examined cast iron was based on high-nickel austenitic cast iron EN GJSA XNi22.

Table 1
Chemical composition of the experimental cast iron

Composition [wt.%]									CE [%]
C	Si	Ni	Mn	Mg	S	P	Cr	Fe	
2.74	2.27	21.14	1.99	0.05	0.02	0.05	0.00	Balance	4.22

3.2. Thermal analysis

Figure 1 presents the results of Thermo-Calc calculations for the investigated alloy system in the phase fraction–temperature representation. The alloy corresponds to a slightly hypoeutectic composition, one in which alloyed austenite (FCC_A1) is the first phase to crystallize at a temperature of 1236.9°C. The equilibrium eutectic solidification temperature is 1207.8°C. Thermo-Calc predictions indicate the presence of graphite at a level of approximately 10 vol.% within the alloyed austenitic matrix, which, as shown later, is consistent with the experimentally observed microstructure.

The recorded cooling curves are shown in Figure 2a, while the cooling rates and solidification time are presented in Figure 2b. The remaining crystallization parameters, determined on the basis of thermal analysis, are summarized in Table 2.

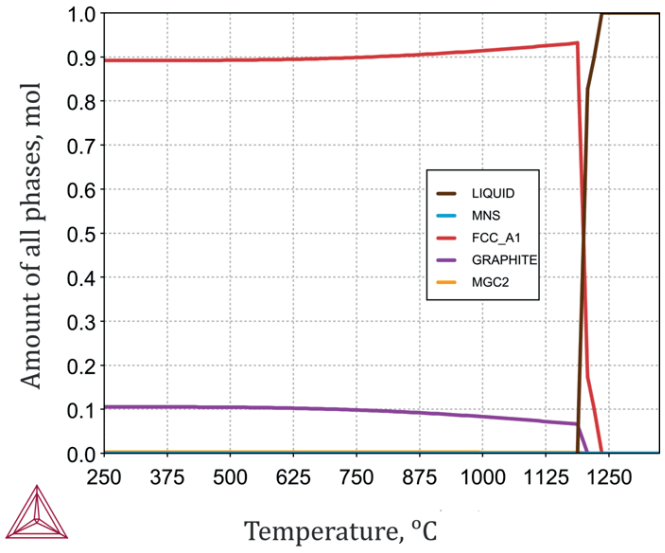

Fig. 1. Amount of phases vs temperature based on Thermo-Calc calculations

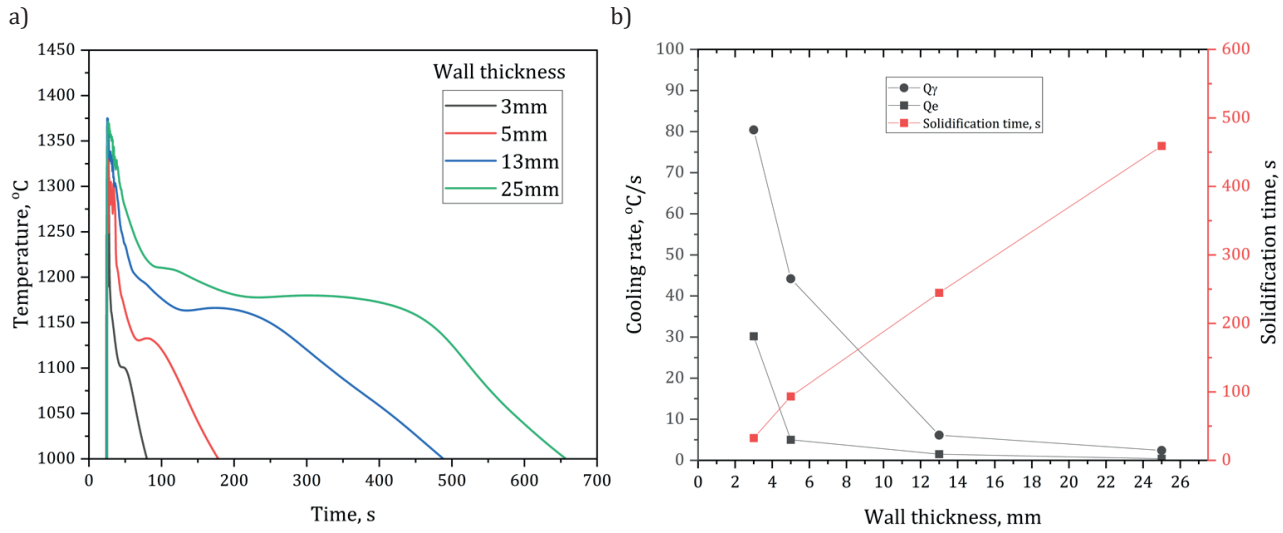

Fig. 2. Cooling curves (a) and cooling rates and solidification time (b) as a function of casting wall thickness

Table 2
Crystallization parameters from the recorded cooling curves

Casting wall thickness [mm]	3	5	13	25
Crystallization start [s]	29.9	41.9	56.7	62.2
Eutectic crystallization start [s]	35.8	49.4	104.2	166.3
Crystallization end [s]	62.3	135.1	301.3	521.2
Crystallization duration [s]	32.5	93.3	244.6	459.1
Eutectic crystallization duration [s]	26.6	85.7	197.1	355.0
Minimal temperature at the beginning of eutectic crystallization T_{min} [°C]	1100.9	1130.4	1163.3	1177.7
Minimal temperature at the beginning of alloy crystallization T_{min} [°C]	1159.6	1176.4	1194.5	1210.7
T_{max} [°C]	1159.6	1132.7	1166.2	1179.9
Recalescence [°C]	0	2.3	2.9	2.1
Cooling rate Q_γ* [°C/s]	80.4	44.2	6.13	2.4
Cooling rate Q_e** [°C/s]	30.2	5.0	1.5	0.4

* Q_γ represents the cooling rate of ductile iron in the vicinity of the equilibrium solidification temperature, estimated on the basis of Thermo-Calc calculations, i.e., at 1236.9°C.

** Q_e represents the cooling rate of ductile iron near the equilibrium graphite eutectic solidification temperature, also estimated from Thermo-Calc calculations, i.e., at 1207.8°C.

The results of the thermal analysis indicate a pronounced effect of casting wall thickness on the cooling rates achieved by the alloy at the onset of solidification, as well as on the solidification time (Fig. 2b). Entering the thin-walled casting regime ($g \leq 5$ mm) is accompanied by a significant increase in the cooling rate[1] (Fig. 1b). An exponential increase in the cooling rate was observed with decreasing wall thickness, manifested by a several-fold rise when the wall thickness was reduced from 13 mm to 5 mm. Thermal analysis also enabled the determination of the solidification time, which exhibits a linear dependence on wall thickness over the entire investigated range, with a high coefficient of determination[2] ($R^2 = 0.99$).

3.3. Microstructures

The microstructure photographs at a magnification 100× are presented in Figure 3. All of the microstructures consist of graphite in the shape of nodules and an austenitic metallic matrix. Importantly, it also shows that, across all of the tested wall thicknesses: 3–25 mm, a high-quality microstructure can be achieved without chills and other structural defects like chunky or clustered graphite particles. Across the entire range of casting wall thicknesses, the graphite volume fraction varied between 7.4 and 8.5 vol.%. The average diameter of the graphite nodules in thin-walled castings was 13.9 μm and increased to 19.6 μm for the casting with the largest investigated wall

[1] The dependences of the casting wall thickness on the cooling rates Q_γ and Q_e can be described using a nonlinear function $y = a - bc^x$. For Q_γ, the fitted parameters are $a = 2.47$, $b = -198.12$, and $c = 0.73$ with a reduced chi-square value of 0.066 and coefficient of determination, $R^2 = 0.99$. For Q_e, the fitted parameters are $a = 0.95$, $b = -567.31$, and $c = 0.37$ with a reduced chi-square value of 0.60 and coefficient of determination $R^2 = 0.99$.
[2] The relationship between the solidification time and the casting wall thickness can be described using a linear function $y = a + bx$, with fitted parameters $a = -11.17$ and $b = 19.00$, and is characterized by a coefficient of determination $R^2 = 0.99$.

thickness. A high degree of nodularity, ranging from 90.2% to 92.0%, was obtained for all of the examined castings. The relationship between the number of graphite nodules and casting wall thickness is presented in Figure 4, together with the fitted curve and a high coefficient of determination (R^2 = 0.966).

The relationship between the graphite nodule count and the casting wall thickness is presented in Figure 4a, together with the fitted curve and the corresponding equation, yielding a high coefficient of determination (R^2 = 0.966). In general, with increasing wall thickness the number of graphite nodules decreases while their diameter increases. Figure 3b illustrates an exponential relationship between the graphite nodule count and the maximum undercooling with respect to the equilibrium eutectic solidification temperature.

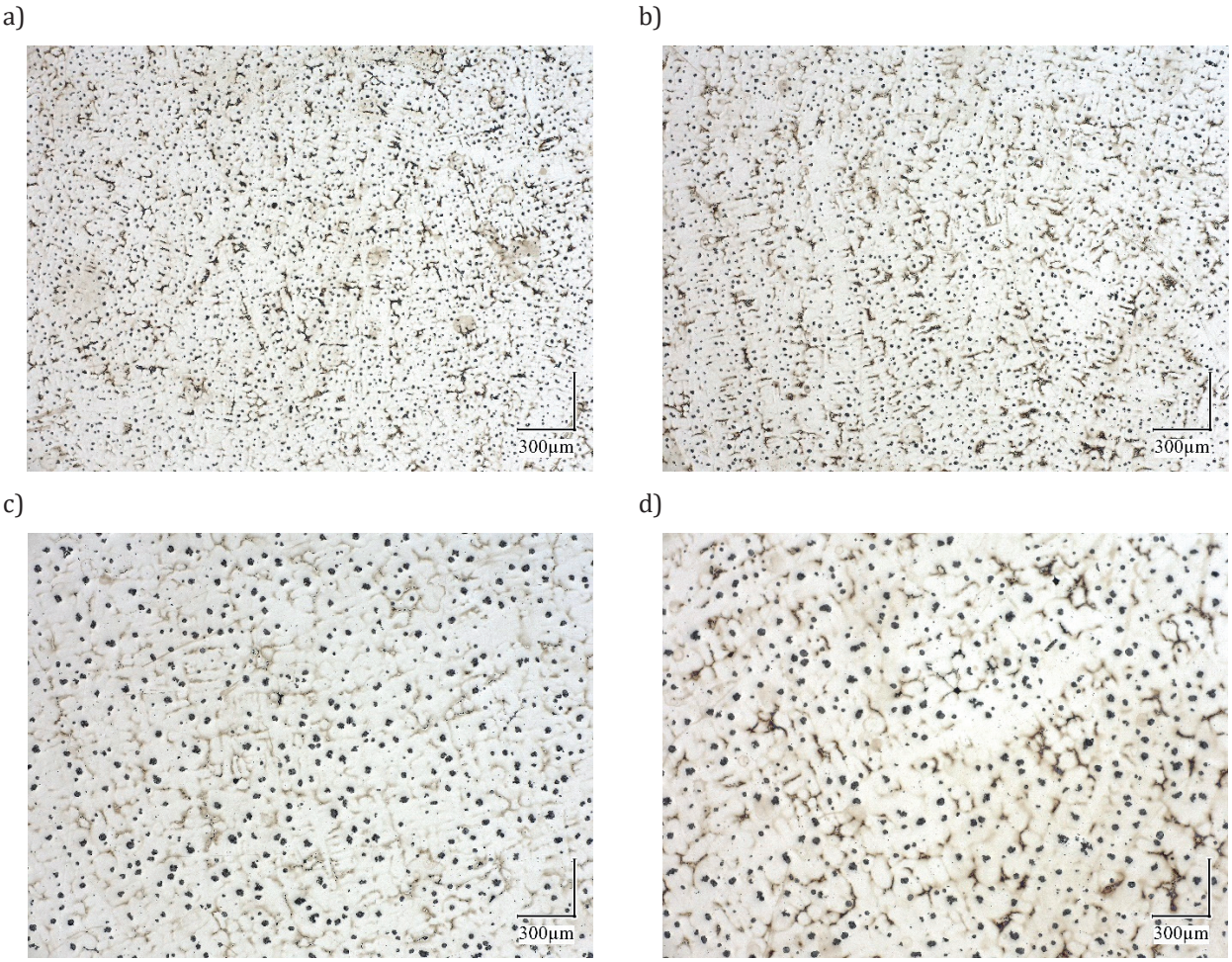

Fig. 3. Microstructures in castings with different wall thickness: a) g = 3 mm; b) g = 5 mm; c) g = 13 mm; d) g = 25mm. Stead etched

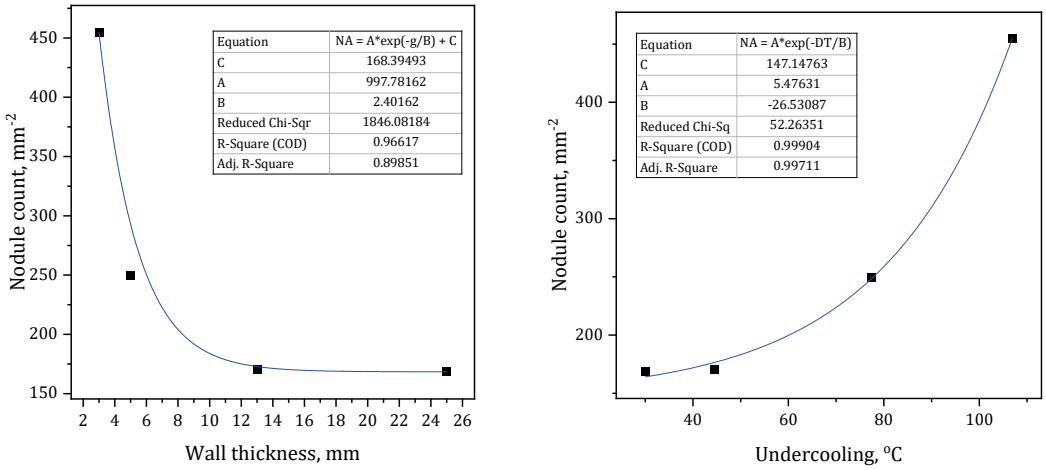

Fig. 4. Graphite nodule count as a function of wall thickness (a) and maximum undercooling below the equilibrium eutectic solidification temperature (b)

Figure 5 shows the effect of wall thickness on the secondary dendrite arm spacing (SDAS) as well as on the number of grains (dendrites) per unit length.

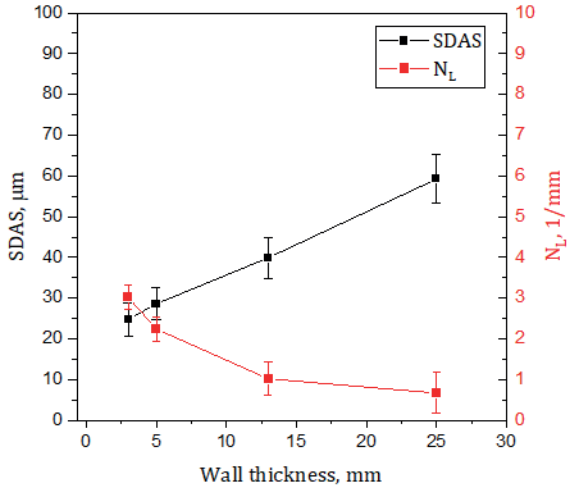

Fig. 5. Secondary dendrite arm spacing (SDAS) as well as the number of grains (dendrites) per unit length vs wall thickness

The grain morphology in thin plate castings is not governed by wall thickness alone, but by the balance between thermal gradient and solidification front velocity, which in sand molds may still favor columnar growth. Directional solidification in the analyzed case is further promoted by the fact that heat is extracted predominantly through the two opposite mold walls. The low thermal conductivity of the furan-based molding sand limits heat dissipation through the bulk of the mold. As a result, intensive melt convection is suppressed, and the solidification front advances in a stable and directional manner from the mold walls toward the center of the casting. Considering the quantitative parameters related to dendritic morphology, the secondary dendrite arm spacing can be described by a linear relationship[3], whereas the number of grains (dendrites) follows an exponential dependence[4] related to the casting wall thickness.

3.4. Tensile test

The results from the static tensile tests are summarized in Figure 6. All of the measured values are in accordance with values required by cast iron grade EN GJSA XNi22, based on which the chemical composition was selected.

It can be concluded that, despite the substantial variations in cooling rates associated with wall thicknesses ranging from 3 mm to 25 mm, the examined ductile iron exhibits relatively low sensitivity to cooling rate, as evidenced by its mechanical properties. Within the investigated wall thickness range, the differences in tensile strength, yield strength, and elongation were limited to ΔR_m = 23 MPa, $\Delta R_{p0.2}$ = 37 MPa, and ΔA = 4%, respectively. This confirms the applicability of the investigated cast iron grade for components with complex geometries, including changing wall thicknesses.

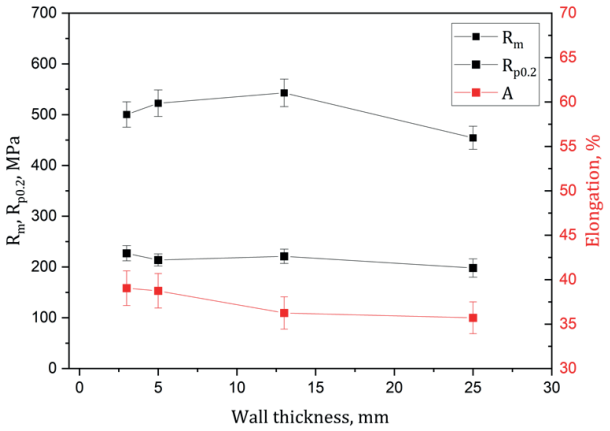

Fig. 6. Summary of results from static tensile test

4. CONCLUSIONS

Based on the conducted investigations on high-nickel austenitic ductile iron EN GJSA XNi22 castings with wall thicknesses ranging from 3 mm to 25 mm, the following conclusions can be drawn:

1. Sound castings free of chills and structural defects can be successfully produced over a wide range of wall thicknesses (3–25 mm). All of the examined sections exhibited a fully austenitic matrix with uniformly distributed spheroidal graphite, characterized by a high nodularity exceeding 90%.
2. Casting wall thickness has a pronounced effect on graphite morphology, particularly on the graphite nodule count and mean nodule diameter. A decrease in wall thickness leads to higher cooling rates, resulting in a significant increase in graphite nodule density and a reduction in nodule size, while the overall graphite volume fraction remains nearly constant (7.4–8.5 vol.%).
3. Thermal analysis revealed an exponential increase in cooling rate with decreasing wall thickness, especially under the thin-walled regime (≤5 mm), accompanied by a strong correlation between maximum undercooling and graphite nodule count. At the same time, solidification time increases nearly linearly with increasing wall thickness.
4. Despite substantial differences in cooling rates and the number of graphite nodules, the investigated austenitic ductile iron exhibits low section sensitivity in terms of mechanical properties. Within the analyzed wall thickness range, the variations in ultimate tensile strength, yield strength, and elongation were limited to ΔR_m = 23 MPa, $\Delta R_{p0.2}$ = 37 MPa, and ΔA = 4%, respectively.
5. The results obtained confirm that EN-GJSA-XNi22 austenitic ductile iron is well suited for complex castings with variable wall thickness, including thin-walled sections, while maintaining stable mechanical performance and high ductility close to 40%.

ACKNOWLEDGMENTS

This research was conducted within the Horizon Europe Project No. 101159771 — NetCastPL4.0.

[3] The relationship between the SDAS and the casting wall thickness can be described using a linear function $y = a + bx$, with fitted parameters a = 20.31, b = 1.55 and is characterized by a coefficient of determination R^2 = 0.99.

[4] The dependence of the casting wall thickness on the number of grains can be described using a nonlinear function $y = a - bc^x$. The fitted parameters are a = 0.64, b = –4.18, and c = 0.83 with a reduced chi-square value of 0.001 and coefficient of determination, R^2 = 0.99.

REFERENCES

[1] American Foundrymen's Society. (1993). *Ductile Iron Handbook*. 2nd Edition. Des Plaines: American Foundrymen's Society.

[2] Rashidi M.M. & Idris M.H. (2014). The effects of solidification on the microstructure and mechanical properties of modified ductile Ni-Resist iron with a high manganese content. *Materials Science and Engineering A*, 597, 395–407. DOI: https://doi.org/10.1016/j.msea.2013.12.070.

[3] Rashidi M.M. & Idris M.H. (2013). Microstructure and mechanical properties of modified ductile Ni-resist with higher manganese content. *Materials Science and Engineering A*, 574, 226–234. DOI: https://doi.org/10.1016/j.msea.2013.02.038.

[4] Moe G. (2022). *Properties and Applications of Ni-Resist and Ductile Ni-Resist Alloys*. 2nd Edition. Durham: Nickel Institute.

[5] Bork M., Górny M., Gondek Ł., Morgiel J. & Morgiel K. (2025). The evaluation of thermal stability, electrical conductivity, and carbide morphology of austenitic ductile iron castings. *Materials*, 18(20), 4734. DOI: https://doi.org/10.3390/ma18204734.

[6] Fragassa C., Radovic N., Pavlovic A. & Minak G. (2016). Comparison of mechanical properties in compacted and spheroidal graphite irons. *Tribology in Industry*, 38(1), 45–56. URL: /www.tribology.rs/journals/2016/2016-1/5.pdf. [15.12.2025].

[7] Fatahalla N., AbuEl-Ezz A. & Semeida M. (2009). Si and Ni as alloying elements to vary carbon equivalent of austenitic ductile cast iron: microstructure and mechanical properties. *Materials Science and Engineering A*, 504(1–2), 81–89. DOI: https://doi.org/10.1016/j.msea.2008.10.019.